# Green Chemistry

Accepted Manuscript






ROYAL SOCIETY OF CHEMISTRY

www.rsc.org/greenchem

Journal Name

RSCPublishing

ARTICLE

# Low content Au-based catalyst for hydrochlorination of $C_2H_2$ and its industial scale-up for future PVC process

Cite this: DOI: 10.1039/xoxxoooooox

Received ooth January 2012,
Accepted ooth January 2012

DOI: 10.1039/xoxxoooooox

www.rsc.org/

Kai Zhou,[a] Jinchao Jia,[a] Chunhua Li,[b] Hao Xu,[a] Jun Zhou,[b] Guohua Luo,[a,*] and Fei Wei,[a,*]

China has the world's largest polyvinyl chloride (PVC) production capacity, comprising over 20 $Mt \cdot a^{-1}$ and occupying 41% of the world production capacity. However, the production of PVC monomer, vinyl chloride monomer (VCM), faces unsustainable development due to mercury problems. Over 70% of VCM in mainland China is synthesized through hydrochlorination of $C_2H_2$ catalyzed by $HgCl_2$. Mercury and its compounds escaping from the reactors have high chronic toxicity, which is harmful to the environment and to people's health. Therefore, developing a novel mercury-free catalyst is crucial to maintaining a green production of PVC in China. This paper shows a novel low content Au-based catalyst by complexing Au with thiocyanate (–SCN). This chemical complex significantly decreases the electrode potential of $Au^{3+}$ from 0.926 V to 0.662 V, and hence reduces the probability of its reduction by $C_2H_2$. The catalyst preserves a high turnover frequency of 5.9 $s^{-1}$ based on Au, and over 3000 hrs test of 4 $t \cdot a^{-1}$ pilot-trial shows its promising reactivity (>95%) and selectivity (>99%). Comparing with the conventional $HgCl_2$ catalyst, this novel Au catalyst has better reactivity, stability, environmental friendliness and lower toxicity, making it promising for the sustainable development of China's PVC industry.

## Introduction

Polyvinyl chloride (PVC) is the second-most widely used general resin because of its advanced features. The production capacity of PVC increases 5.8% per year globally,[1] while in China the capacity has been increasing over 10% annually since 2003 (**Fig. S1(a)**). Two methods are currently employed industrially to produce PVC's monomer, vinyl chloride monomer (VCM). One is pyrolysis of dichloroethane which is synthesized through additional reaction between $C_2H_4$ and $Cl_2$ (**Fig. S2**). The other is called calcium carbide method through hydrochlorination of $C_2H_2$ catalyzed by $HgCl_2$:

$$C_2H_2 + HCl \rightarrow CH_2{=}CHCl \quad \Delta H{=}{-}124.8\ kJ \cdot mol^{-1}$$

**Fig. S3** showed that the global net PVC production capacity is 50.9 $Mt \cdot a^{-1}$ in 2012, of which China holds a 41% share. As the world's largest PVC producing country, China has over 13 $Mt \cdot a^{-1}$ PVC synthesized from calcium carbide method,[2] and this route dominates more than 70% yield (**Fig. S1(b)**). Due to low heat transfer efficiency in fixed bed reactors, hot spots over 200 ºC are easily formed, hence accelerating high volatile mercuric chloride run-off. It is estimated that to produce 1.0 t of PVC consumes 1.02-1.41 kg $HgCl_2$ catalyst ($HgCl_2$ content: 10-12 wt%), while over 25% $HgCl_2$ fails to be reused during the recycling, causing chronic poisoning. Facing the harmful pollution of $HgCl_2$, the development of novel Hg-free catalysts is extremely urgent for establishing a sustainable PVC industry in China. Recently, green Hg-free catalysts, which are mainly heterogeneous catalysts (*e.g.* Au/C,[3-14] Cu-Bi/$SiO_2$,[15] Au-Cu/C,[16] Au-Co/C,[10] $CN_x$,[17-20] Au-Cu-SCN/C,[21]), have become widely studied for the hydrochlorination of $C_2H_2$ process.

Over the past centuries, gold has been valued as a symbol of wealth for its rareness and seeming inertness. Thus, the discovery that gold is an active promoter of many fundamental reactions has excited numerous researchers. Gold, in a cationic form ($Au^{3+}$/$Au^{+}$) is electrophilic and active for nucleophilic attack. Gold cations coordinate preferentially to alkenes or alkynes, making it possible to catalyze all related kinds of reactions ranging from partial oxidation of hydrocarbons to the hydrogenation of unsaturated carbonyl compounds under appropriate conditions,[8, 22-24] such as the oxidation of $CH_4$ and CO, water gas shift, methanol esterification, olefin hydrogenation and hydrochlorination et al. [5, 7, 11, 25-31] Therefore Au has great potential for energy-efficient green chemistry applications,[32-34] like hydrochlorination of $C_2H_2$ to produce VCM. After comparing the catalytic activity of certain kinds of metal chlorides catalysts,[11, 13, 14, 35-38] Hutchings' group has already found that $AuCl_3$ possesses the best reactivity. Thereafter, highly efficient catalysts in the form of Au/C[3-7] were reported and the feasibility was proved to substitute toxic $HgCl_2$ catalysts.

However, the present noble-metal catalysts still faced great challenges for industrial applications, mainly because of their high cost (e.g. 1.0 wt% Au content,[10, 39] shown in **Fig. S4**) and fast deactivation.[40] To overcome these shortages, several ideas were developed, such as adding Cu into the Au catalyst to reduce the Au loading down to 0.5 wt%,[16] or co-feeding oxidizing gas like NO with the reactants to eliminate the deactivation. Although significant improvement has been achieved, the balance between Au loading and reactivity remains unreached.

Meanwhile, Hg-free non-precious metal catalysts have been investigated for decades in the academic field. Mono-metal catalyst $SnCl_2$/C or bimetallic catalyst $BiCl_3$-$CuCl_2$/$SiO_2$ and ternary metal catalyst $SnCl_2$-$BiCl_3$-CuCl/C have acceptable conversion and selectivity;[41-43] Unfortunately, the higher volatility and more severe coke than $HgCl_2$ terminate their industrial applications.

In addition, N-doped carbon materials have been proved to be efficient catalysts for this process recently;[19] however, the industrial scale-up needs further research. In summary, it is expected to create a novel and more efficient nanostructured catalyst, which embodies a balance of economy, activity, selectivity and stability for challenging industrialized applications of green catalysis. Au, as a biocompatible non-toxic metal with outstanding properties, can be molded upon novel hydrochlorination process so long as loading is further lower than present level of 0.5 wt%.

Here we reported a novel Au-complexing catalyst with thiocyanate (–SCN) for hydrochlorination of $C_2H_2$ with 0.25 wt% Au loading. The cost of Au-complexing catalyst was only approximately 25% of Hutching's catalyst, made it comparable with the cost of $HgCl_2$/C and cheap enough for industrial use. The reason for introducing –SCN as a complexing ligand is that the electric potential of $Au(SCN)_4^-$ (0.662 V) is significantly lower than the similar $AuCl_4^-$ (0.926 V) or $AuBr_4^-$ (0.802 V) as shown in **Table 1**; therefore the reduction rate of $Au^{3+}$ to $Au^0$ by $C_2H_2$ can be significantly slowed down. It should be noted that although the $Au(CN)_2^-$ has the lowest electric potential, its fatal toxicity forbids its use in this system. Compared with –CN, –SCN and its related compounds have lower toxicity and better environmental friendliness, which can be applied in large quantities.

Experimental results and density functional theory (DFT) study indicates that the reduction of $Au^{3+}$ is the main factor of deactivation, and the combination of –SCN and Au protects $Au^{3+}$ from reduction by $C_2H_2$. Pilot-trial on a scale of 4 $t \cdot a^{-1}$ has operated over 3000 hrs and shows satisfactorily high reactivity (>95%) and selectivity (>99%) of VCM under gas hourly space velocity (GHSV, $C_2H_2$ based) of 30 $h^{-1}$, a big step for future industrial applications.

**Table 1.** Related half-reactions and corresponding electric potential of Au-complexing ions.

| Half-reaction | Electric potential (V) |
|---|---|
| $Au^{3+} + 3e^- = Au$ | 1.520 |
| $AuCl_4^- + 2e^- = AuCl_2^- + 2Cl^-$ | 0.926 |
| $AuBr_4^- + 2e^- = AuBr_2^- + 2Br^-$ | 0.802 |
| $Au(SCN)_4^- + 2e^- = Au(SCN)_2^- + 2SCN^-$ | 0.623 |
| $Au(SCN)_4^- + 3e^- = Au + 4SCN^-$ | 0.662 |
| $AuBr_2^- + e^- = Au + 2Br^-$ | 0.960 |
| $AuI_2^- + e^- = Au + 2I^-$ | 0.576 |
| $Au(CN)_2^- + e^- = Au + 2CN^-$ | -0.596 |
| $Au(SCN)_2^- + e^- = Au + 2SCN^-$ | 0.69 |

## Results and discussion

### Lab-scale analysis

All tested catalysts' name, chemical composition, deactivation rate, selectivity and test time were collected in **Table 2**. The catalyst loading 0.50 wt% Au with $HAuCl_4$ as active precursor was named as *Catal. A*. The catalyst loading 0.50 wt% Au and 0.50 wt% KSCN with $HAuCl_4$ and KSCN as precursors was abbreviated as *Catal. AS*. The catalyst with $HAuCl_4$, KSCN and $CuCl_2$ as precursors was noted as *Catal. ACS*, and Au loading was according to prefix description. The catalyst with $HAuCl_4$, KCl and $CuCl_2$ as precursors was called *Catal. ACK* (n(Au):n(Cu):n(K)=1:5:20, Au loading was 0.25 wt%). The catalyst with $HAuCl_4$ and $CuCl_2$ as precursors was named as *Catal. AC* (n(Au):n(Cu)=1:5, Au loading was 0.25 wt%). All the catalysts were prepared by incipient-wetness impregnation method.

**Table 2.** Characterizations of composition and reactivity performance in all catalysts (T=180 ºC).

| Catalyst name | Chemical Composition | Deactivation rate (%·min$^{-1}$)[‡] | Selectivity (%) | GHSV ($h^{-1}$) |
|---|---|---|---|---|
| *Catal.A* | 0.50 wt% Au | 0.047 | >99 | 1200 |
| *Catal.AS* | 0.50 wt% Au<br>0.50 wt% KSCN | - | >99 | 1200 |
| *Catal.ACS*[†] | 0.25 wt% Au<br>1.62 wt% Cu<br>2.46 wt% KSCN | 0.014<br>0.008 | >99 | 1200<br>360 |
| *Catal.ACK* | 0.25 wt% Au<br>1.62 wt% Cu<br>1.89 wt% KCl | 0.015 | >99 | 360 |
| *Catal.AC* | 0.25 wt% Au<br>1.62 wt% Cu | 0.017 | >99 | 360 |

[†] We only give composition of the optimized *Catal. ACS* here due to too many compositions in optimization.

[‡] Deactivation rate is defined to be the value of the loss of conversion per minute during deactivation stage, which is 'r=-ΔConversion (%)/Δt (min)'.

**Fig. 1(a)** showed that *Catal. A* had good initial reactivity (40%) but too high deactivation rate (0.047 %·min$^{-1}$). After coordination of –SCN, *Catal. AS* performed poorer initial reactivity (36%) but more promising stability than *Catal. A*, indicating actual promotion of –SCN in catalytic reactivity. To promote catalytic performance of Au catalyst, Cu was introduced into this system.[44, 45] The optimized ratio of Cu:Au was determined by reactivity analysis as shown in **Fig. 1(b)**. When ratio of n(Cu):n(Au) increased from 0:1 to 5:1, the reactivity was the best at n(Cu):n(Au)= 5:1; However, with a ratio higher than 5:1, no apparent reactivity increase was observed. Because catalyst with n(Cu):n(Au)=5:1 had relatively lower deactivation rate, 5:1 was selected as the optimized ratio in the following evaluation. The optimization of –SCN content was also implemented by increasing the ratio of n(SCN):n(Au) from 0:1 to 40:1. As shown in **Fig. 1(c)**, when the ratio

increased from 0:1 to 20:1, –SCN had significant effect in preserving reactivity; however, no notable promotion was found when the ratio continued increasing (**Fig. S5**), and a ratio of 20:1 was selected to be the best value. Au loading was also investigated. The conversion of $C_2H_2$ decreased accompanied with the decreasing Au content but the 0.25 wt% *Catal. ACS* (0.014 %·min$^{-1}$) had similar deactivation rate with 0.50 wt% *Catal. ACS* (0.013 %·min$^{-1}$) and higher conversion than 0.10 wt% *Catal. ACS*. Comprehensively, 0.25 wt% *Catal. ACS* was selected as the optimized catalyst for our reaction system, abbreviated as *Catal. ACS* (0.25 wt% Au, n(Au):n(Cu):n(SCN)=1:5:20) in the next narration.

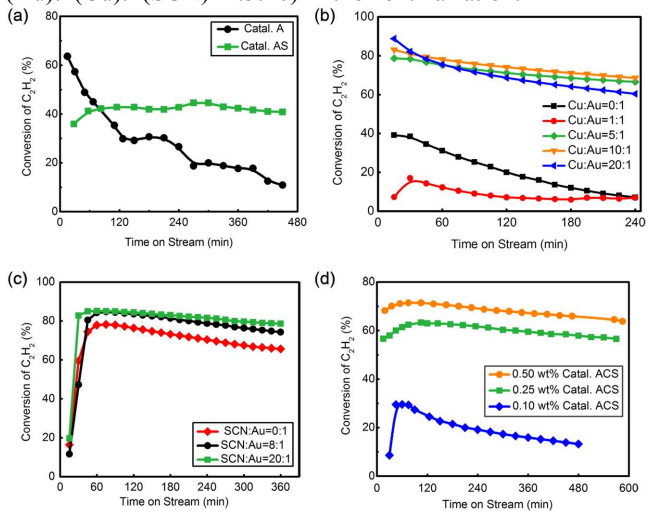


**Figure 1**. **(a)** The reactivity evaluation of *Catal. A* and *Catal. AS* (0.50 wt% Au content); **(b)** The reactivity evaluation of Au-Cu series catalysts (0.50 wt%) with various mole ratio of n(Cu):n(Au)=1:1, 5:1, 10:1 and 20:1; **(c)** The reactivity evaluation of *Catal. ACS* (0.50 wt% Au, n(Cu):n(Au)=5:1) with various mole ratio of SCN:Au=0:1, 8:1 and 20:1; **(d)** The reactivity evaluation of *Catal. ACS* with different Au content: 0.50 wt%, 0.25 wt% and 0.10 wt%. All evaluations were operated at 180 °C and GHSV of 1200 h$^{-1}$.

Transmission electron microscopy (TEM) characterization (**Fig. S6(a)**) showed that the detected particles in *Catal. ACS* were almost smaller than 10 nm, and X-ray diffraction (XRD) patterns (**Fig. S10(c)**) of fresh catalyst had no visible diffraction peaks of crystals, supposing good dispersion of active components. Scanning electron microscopy (SEM) image in **Fig. S6(b)** was in good agreement with TEM and XRD detection. It has been confirmed that the introduction of Cu facilitates the dispersion of Au previously.[44-46] The above characterizations well demonstrated that the employment of thiocyanate (–SCN) had no negative influence on ions dispersion.

Three catalysts, which were *Catal. ACS*, *Catal. ACK* and *Catal. AC*, were evaluated to test their catalytic reactivity. 10 hrs' test in **Fig. 2(a)** showed that *Catal. ACS* had the lowest deactivation rate. The K had no apparent effect in inhibiting deactivation, but –SCN had a significant role in reactivity preservation. To find the state changes of Au in the catalyst, X-ray photoelectron spectroscopy (XPS, ESCALAB 250Xi, Al Kα source) was systematically employed. The XPS data of Au was well fitted by decomposing the spectrum into Au $4f_{5/2}$ and Au $4f_{7/2}$ peaks. The binding energies at 89.8 ± 0.1 eV and 86.4 ± 0.1 eV were attributed to the $Au^{3+}$ oxidation states, and those at 87.6±0.1 eV and 83.9±0.1 eV were attributed to the $Au^0$ metal states.[47-49] The amount of $Au^+$ species was neglected because no observed peaks belonged to $Au^+$ species. The most important feature of the XPS spectra was possibly that, in the preparation, small metallic gold clusters (hereafter labelled $Au^0$-s) were also formed, the binding energy of which was *ca.* 1 eV higher than the Au 4f binding energy of the majority of the $Au^0$ species.[48, 50] However, we considered the $Au^0$-s species to be nothing more than a spectator species, since the reduced catalysts also contained these $Au^0$-s nano-clusters and were inactive. **Fig. 2(b)** showed that the fresh *Catal. ACS* possessed more $Au^{3+}$, and as the catalyst became inactive, $Au^{3+}$ generally transformed into $Au^0$ or $Au^0$-s by reduction. Quantification of the Au species on 3 catalysts' surface was given by integrating the corresponding peaks area of Au $4f_{7/2}$ (**Fig. 2(c)** and **Table S1**). Former study indicated that the reduction of $Au^{3+}$ led to catalyst deactivation,[7, 35] and the positive correlation of $Au^{3+}$ proportion with $C_2H_2$ conversion in *Catal. ACS* here coincided with that. In comparison, *Catal. ACS* (from *ca.* 68% to *ca.* 20%) had better preservation of $Au^{3+}$ than *Catal. AC* (from *ca.* 61% to *ca.* 12%) and *Catal. ACK* (from *ca.* 73% to *ca.* 15%).

BET analysis showed that three catalysts' surface area all decreased after evaluation. The loss of micro surface dominated, which indicated that coke accumulated mainly in micro pores. Similarly, *Catal. ACS* ($S_{micro}$ from 663.8 $m^2 \cdot g^{-1}$ to 600.3 $m^2 \cdot g^{-1}$) had a better anti-coke ability than *Catal. AC* ($S_{micro}$ from 768.9 $m^2 \cdot g^{-1}$ to 596.4 $m^2 \cdot g^{-1}$) and *Catal. ACK* ($S_{micro}$ from 626.3 $m^2 \cdot g^{-1}$ to 489.6 $m^2 \cdot g^{-1}$). The coke rate test further confirmed this conclusion by recording the change of catalysts' weight during the reaction.

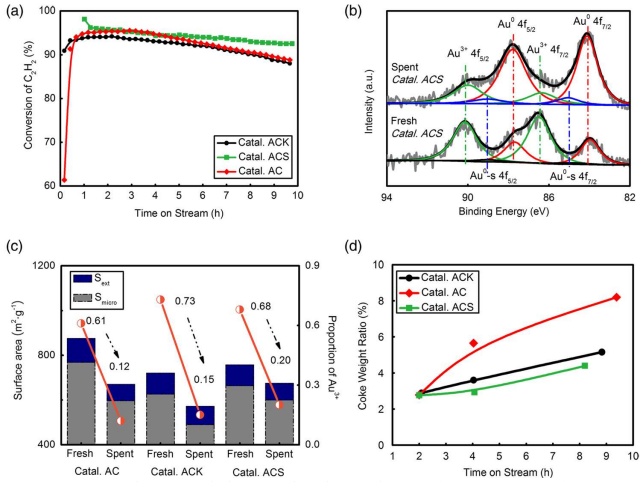


**Figure 2**. **(a)** The reactivity evaluation of *Catal. ACK, Catal.ACS* and *Catal. AC* (0.25 wt% Au content); **(b)** The XPS spectrum of Au in fresh and spent *Catal. ACS*; **(c)** Textural properties of fresh and spent catalysts (*Catal. AC*, *Catal. ACK* and *Catal. ACS*); **(d)** The coke weight ratio in *Catal. AC*, *Catal. ACK* and *Catal. ACS*. (T=180 °C, GHSV=360 h$^{-1}$)

Conventionally, Hg-based catalysts are too volatile to be stabilized in the catalysts over 200 ºC. As a result, thermal stability is considered a very important factor for Hg-free catalysts. Au and Cu in *Catal. ACS* was decided by both inductively coupled plasma optical emission spectrometer (ICP-OES) and XPS analysis. Two metals' content had no apparent changes, proving good thermal stability. The minor difference of metals content between XPS and ICP was attributed to their different distribution tendencies on the surface or in body of substrate (**Table 3**). Au content derived from XPS was relatively lower than that from ICP, which meant that Au preferred to anchor in abundant micro pores rather than on the surface. Cu had similar content in two analysis, showing its uniform loading in catalyst.

**Table 3.** Atomic composition of *Catal. ACS* derived from XPS and ICP data, respectively.

| Measure method | Catalyst type | Au (%) | Cu (%) | K (%) |
|---|---|---|---|---|
| XPS | Fresh Catalyst | 0.16 | 0.41 | 1.11 |
| | Spent Catalyst | 0.15 | 0.41 | 1.05 |
| ICP | Fresh Catalyst | 0.23 | 0.41 | 1.08 |
| | Spent Catalyst | 0.21 | 0.40 | 0.97 |

Experiment results showed good catalytic promotion of –SCN; however, its mechanism needed further studying. XPS measurement was conducted to check the S species. As shown in **Fig. S7**, the binding energy of –R-S in *Catal. ACS* (163.0 eV) was 0.5 eV higher than that in KSCN (162.5 eV), [51-53] which might be attributed to the electron transfer from S to Au. To exclude the possible effect of $S^{2-}$, catalyst in the name of *Catal. ACS'* (0.25 wt% Au, $n(HAuCl_4):n(CuCl_2):n(Na_2S)=1:5:20$) was employed for comparison. As shown in **Fig. S8**, *Catal. ACS'* had poorer reactivity and stability than *Catal. ACS*, which confirmed the conclusion that the interaction of –SCN and Au improved the reactivity performance.

Detailed DFT study was also conducted here to discuss the role of –SCN in reactivity preservation. Jinli Zhang et al[40] studied the reaction and deactivation mechanism of $Au_2Cl_6$ and speculated that reduction of $Au^{3+}$ from $C_2H_2$ might be the key factor of deactivation. Therefore, we compared the reduction possibility of $Au_2Cl_6$ and $Au_2Cl_5$-SCN, where the latter one was thought to be the primary structure of complexing. Two reaction paths for $C_2H_2$ hydrochlorination were shown in **Fig. 3**. $Au_2Cl_6/Au_2Cl_5$-SCN and $C_2H_2$ without any interaction were chosen as the initial state. As $C_2H_2$ moved closely towards $Au_2Cl_6/Au_2Cl_5$-SCN, C atom in $C_2H_2$ began to interact with Cl in $Au_2Cl_6/Au_2Cl_5$-SCN. The stable adsorption structures of $C_2H_2$–$Au_2Cl_6/Au_2Cl_5$-SCN were defined to be reactants 'R'. It should be noted that $C_2H_2$ preferred to interact with Cl atom at top position in the $Au_2Cl_5$-SCN (**Fig. S9(a)**) and with Cl at side in the $Au_2Cl_6$ (**Fig. S9(b)**). The energy also showed a slight difference between each other: $C_2H_2$–$Au_2Cl_5$-SCN (8.01 kcal·mol$^{-1}$) was 1.49 kcal·mol$^{-1}$ higher than $C_2H_2$–$Au_2Cl_6$ (6.52 kcal·mol$^{-1}$). As C in the $C_2H_2$ went on interacting with Au catalyst, it derived Cl atom and formed bonds with it, which was called products 'P'. The 'Final State' was referred to the desorbed hydrocarbon derivatives and deactivated catalyst without any interaction. The transition state 'TS' showed that the energy of $C_2H_2$–$Au_2Cl_5$-SCN (**Fig. S9(c)**, 37.22 kcal·mol$^{-1}$) was 4.19 kcal·mol$^{-1}$ higher than $C_2H_2$–$Au_2Cl_6$ (**Fig. S9(d)**, 33.03 kcal·mol$^{-1}$), which could not be ignored. Besides, the energy barrier (energy between 'TS' and 'R') in $C_2H_2$–$Au_2Cl_5$-SCN was 2.7 kcal·mol$^{-1}$ higher than that in $C_2H_2$–$Au_2Cl_6$, proving less possibility of SCN-complexing catalyst to deactivate. Having significant steric effects and similar chemical properties as halogen might be the reason why –SCN had better stability promotion than –Cl. We could imagine that when Au complexed with more –SCN, it would possess more anti-reduction ability. The detailed energy change in this DFT study was listed in **Table S3** and **Table S4**. DFT study showed promising effect in anti-reduction by $C_2H_2$, however other promotion of SCN-complexing in anti-deactivation should be further studied.

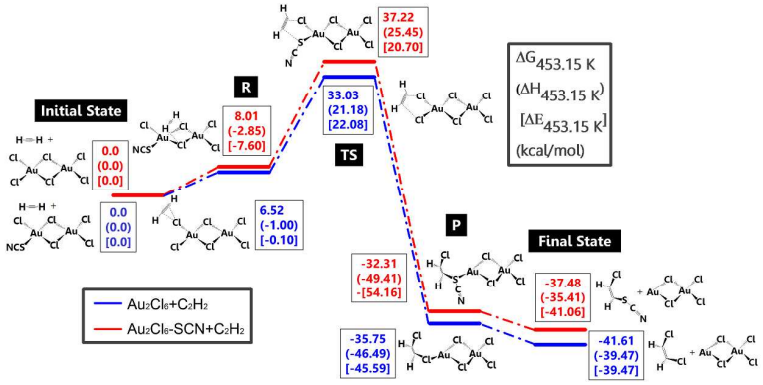


**Figure 3**. DFT calculated energy surface for $C_2H_2$ reduction with $Au_2Cl_6$ and $Au_2Cl_5$-SCN.

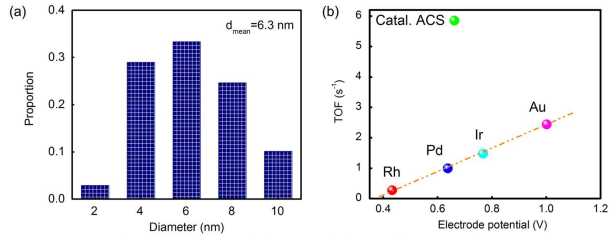


**Figure 4. (a)** The statistics of the particles' diameter in *Catal. ACS*; **(b)** Correlation between initial $C_2H_2$ conversions versus the standard electrode potential of *Catal. ACS* and other various metals.[38] Potentials are obtained from the reduction potentials of the following chloride salts $(RhCl_6)^{3-}$, $PdCl_2$, $(IrCl_6)^{3-}$ and $(AuCl_4)^-$ to the corresponding metals.

The reactivity of *Catal. ACS* was measured by the value of turnover frequency (TOF). The Au nanoparticles had a mean diameter of 6.3 nm by counting hundreds of particles according to the TEM analysis (See in **Fig. 4(a)**). Following the calculation procedure of Hutchings group' method,[7] the TOF was 5.9 s$^{-1}$, which was different from the linear relationship as **Fig. 4(b)** shown. Although the effect of Cu in activity shouldn't be ignored, its contribution was relatively poor;[3-7] the main role of Cu in promoting catalyst's activity is to promote the dispersion, therefore the calculation excluded the influence Cu.

## Scaling up trial

The industrial performance of *Catal. ACS* was evaluated under 96 kg·a$^{-1}$ and 4 t·a$^{-1}$ scale trials (VCM weight based). In 96 kg·a$^{-1}$ scale fixed bed reactor, 60 g catalyst was synthesized following the same preparation procedures in lab. During 200 hrs' test, the conversion and selectivity were above 95% and 99%, respectively. Three types of spent catalysts in different

locations of reactor, which were upper layer, middle layer and bottom layer (**Fig. S10(a)**), were collected to understand deactivation rule. XRD patterns in **Fig. S10(c)** showed that the peaks indicating Au particles became sharper and higher from bottom to upper layer. Combined with the reactivity evaluation in **Fig. S10(d)**, we could conclude that increasing size of Au particles caused less utilization ratio of Au, which was thought of as a sign of deactivation.

Although the catalyst showed advanced ability in inhibiting coke accumulation, coke might still affect the catalyst performance during the evaluation. The spent catalysts had visible decrease in surface area (**Fig. S11**), while the values from different layers had slight differences, which might be attributed to the limited evaluation time. Hutchings et al[54] tried to verify by-products through collecting reaction products in a chloroform trap at the outlet of the reactor and found haloalkane. However, the coke was not further studied before. To check the coke species, gas chromatography–mass spectrometry (GC-MS) was employed. Cyclohexane was applied as the solvent to soak the crushed catalysts for hours at room temperature. The supernatant was used to quantify the ratio of coke species. As shown in **Fig. S12**, coke in three layers was mainly aromatic hydrocarbon or derivatives of aromatic hydrocarbons. The hydrocarbons containing benzene rings were not so volatile, and it might be accumulated and covered on the surface. In addition, derivatives of aromatic hydrocarbons containing O and N were also found. The oxygen might come from the catalyst or reaction gases. When the feeding gases went through the catalyst layers, the contained O was consumed gradually. The presence of N-contained compounds was thought to be from decomposition of –SCN, a sign of deactivation of the catalyst.

Neither Au-particles growth nor loss of N was direct indication of deactivation. Therefore, to find out a more essential factor of reactivity, a pilot-trial with 4 $t \cdot a^{-1}$ scale was further evaluated. This trial has been running for over 3000 hrs.

The flow chart of the process was shown in **Fig. S13**. 4.6 L catalyst was filled in the single tube fixed bed reactor. Three pipelines deliver $N_2$, HCl and reactant gases ($C_2H_2$ and HCl, $Q(C_2H_2):Q(HCl)=1.0:1.1$ $L \cdot h^{-1}$: $L \cdot h^{-1}$) respectively, and their flow rates are controlled by mass flowmeters. Gases need warming up by going through preheaters before enter into the reactor. The catalyst' temperature is recorded by 13 thermocouples (named as T101-T113) distributed in the reactor with 30 cm distance vertically between each other.

The pre-treatment was operated following drying and activation procedures. $N_2$ and HCl, which played the roles of drying and activation respectively, were fed into the reactor in order under the GHSV of 60 $h^{-1}$ for 4 hrs separately at 130 °C. After that, reaction began and mixed reactant gases were input throughout the catalyst layers under GHSV of 60 $h^{-1}$. During the reaction, the space velocity increased generally from 20 $h^{-1}$ to 30 $h^{-1}$ by increasing the flow rate (**Fig. 5(a)**). After 3000 hrs' evaluation, the conversion was still above 95% and the selectivity tested by flame ionization detector (FID) was always above 99% (**Fig. 5(b)** and **Table S5**), which showed that complexing –SCN enabled the catalyst with long-lifespan and good catalytic performance.

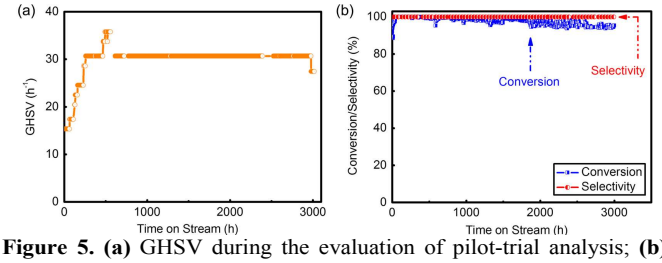


**Figure 5. (a)** GHSV during the evaluation of pilot-trial analysis; **(b)** Conversion and selectivity in this 3000 hrs' evaluation.

During the evaluation, temperatures were recorded in five selected layers, which were T102, T104, T106, T108 and T112 (**Fig. 6(a)** and **(b)**). In the beginning, temperature in layer 1 (labelled as T102) had the highest temperature, and it dropped linearly from 200 ºC. As the reaction continued over 500 hrs, T104 in layer 2 generally went higher than T102 and became the highest. It was found that after 2500 hrs' test, the hot spot shifted to T106, which was in the middle position of the reactor. The catalyst in layer 5 (T112) had the lowest temperature at all times, suggesting less intense reaction in this position. The spent catalysts in five different layers were selected to verify the deactivation rule for hydrochlorination of $C_2H_2$. As shown in **Fig. 6(c)**, the XRD patterns of the spent catalysts were similar to that of the test in fixed bed reactor, which obeyed the conclusion that Au particles grew larger from bottom layer to upper layer. Besides, five spent catalysts had significant difference in reactivity as shown in **Fig. 6(d)**. Under the evaluation conditions of 180 ºC and 360 $h^{-1}$, catalyst in layer 5 had around 40% conversion while the one in layer 1 had only 4% conversion. That was to say catalysts' deactivation went more severe from the bottom to the upper.

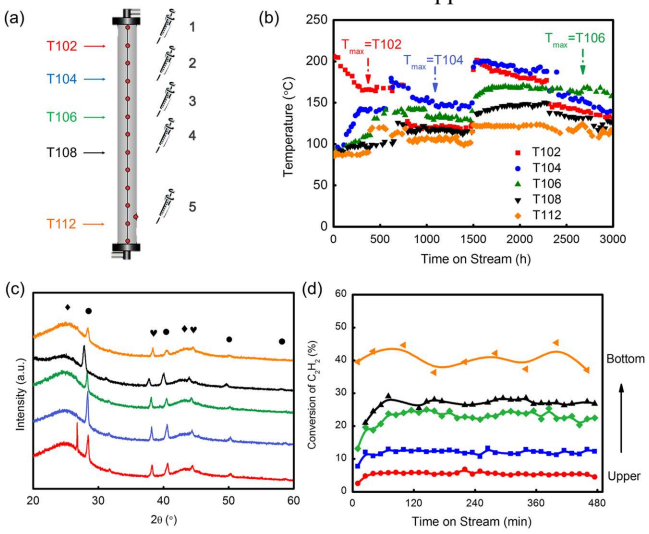


**Figure 6. (a)** The schematic diagram of the positions in reactor for temperature record and catalyst selection; **(b)** Temperature change in reactor during the evaluation; **(c)** XRD patterns of the spent catalysts selected from different layers of the reactor (♦: C; ●: KCl; ♥:Au); **(d)** The reactivity evaluation of the spent catalysts selected from different layers of the reactors. (T=180 ° C and GHSV=360 $h^{-1}$).

BET test showed that the surface area of five spent catalysts (distance of layer 1-5 from the reactor top is 30, 90, 150, 210 and 330 cm, respectively) decreased from layer 5 to layer 1 as shown in **Fig. S14**, but the differences of the values were not significant, showing that the loss of surface area wasn't likely the key factor of deactivation.

Au species of five spent catalysts were quantified by XPS spectrums of Au $4f_{7/2}$, and three species including $Au^0$, $Au^{3+}$ and $Au^0$-s were identified (**Table 4**). The value of $Au^{3+}/(Au^{3+}+Au^0+Au^0\text{-s})$ was defined as $Au^{3+}$ proportion, which increased from catalyst in layer 1 (0.86%) to that in layer 5 (13.0%). ICP analysis, which had good precision, was applied to detect Au content. Repeated analysis showed lower than 5% error with each other, and the Au content was listed in **Table S6**. Using these Au content, the correlation of $Au^{3+}$ content and conversion of $C_2H_2$ were also calculated and listed in **Table S7**. According to the converted $C_2H_2$ and Au content, it was clear that the value of $n(C_2H_2)_{converted}/n(Au^{3+})$ was almost a constant of 3.3 $s^{-1}$, while the value of $n(C_2H_2)_{converted}/n(Au)$ had no such consistency. The unusual data in layer 1 and 2 might be from the low conversion of $C_2H_2$ or un-estimated factors of grain size. It should be noted that the value of $n(C_2H_2)_{converted}/n(Au^{3+})$ was different from the TOF value due to no consideration of particles distribution in its calculation.

**Table 4.** Quantification and identification from XPS of Au species over *Catal. ACS* subject to spent ones in pilot-trials.

| Layer | Species | Position(eV) | Area | $Au^{3+}/(Au^{3+}+Au^0+Au^0\text{-s})$ |
|---|---|---|---|---|
| | $Au^0$ $4f_{7/2}$ | 84.15 | 118.36 | |
| **1** | $Au^{3+}4f_{7/2}$ | 86.52 | 1.2 | 0.86% |
| | $Au^0$-s | 84.93 | 20.22 | |
| | $Au^0$ $4f_{7/2}$ | 84.22 | 183.64 | |
| **2** | $Au^{3+}4f_{7/2}$ | 86.37 | 2.81 | 1.1% |
| | $Au^0$-s | 84.9 | 74.42 | |
| | $Au^{3+}4f_{7/2}$ | 86.42 | 25.63 | |
| **3** | $Au^0$ $4f_{7/2}$ | 84.25 | 226.81 | 8.6% |
| | $Au^0$-s | 84.95 | 38.80 | |
| | $Au^0$ $4f_{7/2}$ | 84.27 | 127.55 | |
| **4** | $Au^{3+}4f_{7/2}$ | 86.5 | 15.43 | 9.3% |
| | $Au^0$-s | 84.95 | 22.40 | |
| | $Au^0$ $4f_{7/2}$ | 84.24 | 310.47 | |
| **5** | $Au^{3+}4f_{7/2}$ | 86.51 | 57.70 | 13.0% |
| | $Au^0$-s | 84.79 | 89.35 | |

Apart from that, $Au^{3+}$ proportion (the $Au^{3+}$ content was nearly the same) was correlated with catalyst positions and conversion of $C_2H_2$. **Fig. 7** showed that both two sets of data had very good linearity, which indicated that $Au^{3+}$ was verisimilarly the most essential factor of reactivity in converting $C_2H_2$ into VCM. However, the conversion of fresh catalyst did not obey the rule (**Fig. 7(b)**); that might be attributed to over-rich $Au^{3+}$ cations. The critical point could be derived from the intersection of extension cord of data points and the line of 100% conversion, which was 36%. That is to say, to totally convert the $C_2H_2$, 36% $Au^{3+}$ is enough in 0.25 wt% *Catal. ACS*. However, it should be noted here that this conclusion was only derived from *Catal. ACS* and may not be suitable to other catalysts as catalysts' accessory ingredients or complexing ligand would together affect their performance. Therefore, possessing high $Au^{3+}$ proportion (68%) in fresh one, the catalyst could continue to reduce the usage of Au to a further low value, which was a very good sign for its applications in chlor-alkali industry.

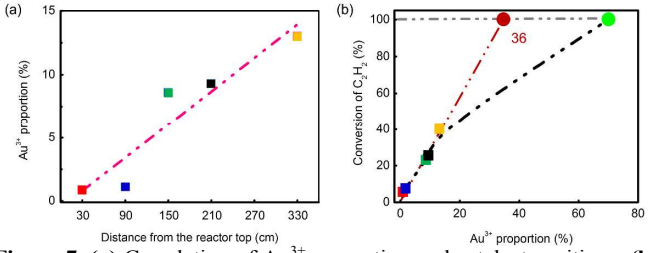


**Figure 7. (a)** Correlation of $Au^{3+}$ proportion and catalyst positions; **(b)** Correlation of $Au^{3+}$ proportion and conversion of $C_2H_2$ (The colored square icons were spent catalysts' data; the green circle icon was fresh catalyst's data with 100% conversion of $C_2H_2$; The scarlet circle icon was the intersection of extension cord of data points and the line of 100% conversion).

## Conclusions

Overall, we have outlined how the outstanding properties of the thiocyanate-complexed Au catalyst, a biocompatible non-toxic metal, can be molded upon new processes based on the hydrochlorination. The optimized catalyst loading of only 0.25 wt% Au has good reactivity and low deactivation rate (0.014 %·$min^{-1}$ at GHSV=1200$h^{-1}$) with a TOF value as high as 5.9 $s^{-1}$. As a complexing ligand, –SCN can interact with Au cations and reduce the electric potential of Au cations significantly from 0.926 V to 0.662 V. DFT study shows that the complexing increases the energy barrier of reaction with $C_2H_2$ and prevent Au catalyst to quick deactivation. As a result, the catalytic reactivity and stability is promoted effectively. The scaling up trial proves that the deactivation is a linear process, the loss of $Au^{3+}$ rather than coke to be the main factor. Over 3000 hrs 4 t·$a^{-1}$ industrial test shows the catalyst' promising performance with >95% conversion and >99% selectivity, which well meets applications in the cholor-alkali industry. The green and efficient catalytic process provides an applicable core-catalyst for sustainable development of PVC in China.

## Experimental

### Catalyst preparation

The catalyst was prepared by impregnation method. $HAuCl_4{\cdot}H_2O$ (M=357.80 g·$mol^{-1}$) and $CuCl_2{\cdot}2H_2O$ (M=170.48 g·$mol^{-1}$, Sinopharm Chemical Reagent Co., Ltd, Beijing) were employed as the precursors of active components. Columnar coconut shell charcoal, one type of carbon, was selected as the catalyst substrate because its abundant surface functional groups can facilitate the dispersion of metal cations. The substrate features in 3 mm in mean diameter, 15 mm in mean length and *ca.* 0.44 g·$mL^{-1}$ in packing density. The complexing ligand (–SCN) supplier in the form of KSCN (M=97.18 g·$mol^{-1}$, Beijing Chemical Works) was introduced to coordinate Au cations.

The typical preparation of the catalyst proceeded as follows. First, carbon substrate was impregnated in aqua regia for 10 hrs, washed with deionized water 3 times and then dried at 120 ºC for 10 hrs as pretreatment for further use. $HAuCl_4 \cdot H_2O$ and $CuCl_2 \cdot 2H_2O$ were weighed *ca.* 0.045 g and 0.268 g respectively and then dissolved in 17.5 mL deionized water to form an aqueous solution. 10 g pretreated carbon substrate was mixed with the aqua solution and 5 mL 0.5 M KSCN solution was added into the mixture dropsies under continuous stirring. The paste formed was ground at 60 ºC for 2 hrs and dried at 120 ºC for 9 hrs in static air. The catalyst was preserved in dry surroundings at room temperature after preparation. To facilitate the evaluation in differential reactors, the catalyst was milled and sieved into 30-60 mesh, with average particle size of 380 μm and packing density of 0.48 $g \cdot mL^{-1}$.

### Catalytic Evaluation

The catalytic behavior was tested in fixed bed reactors in different scales according to the usage of catalyst. As shown in **Fig. 8**, the U-shaped silica tube with a 6mm inner diameter loading 0.15 g catalyst was applied in lab-scale test, the fixed bed reactors with 30 mm and 80 mm inner diameters were applied to load 60 g and 2.5 kg catalyst respectively for progressively scaling-up tests.

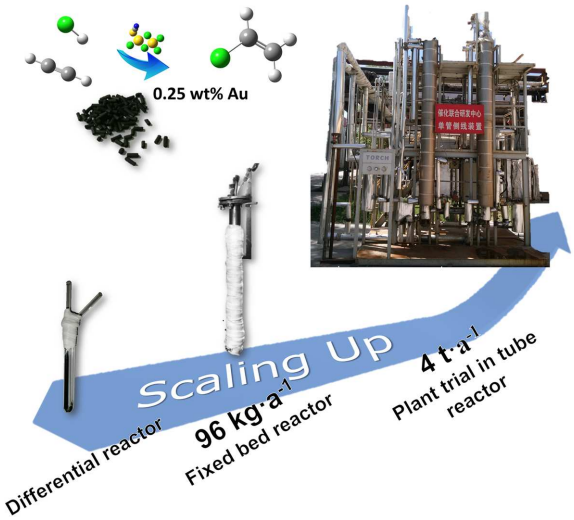


**Figure 8**. The fixed bed reactors in different scales: the U-shaped silica tube with a 6 mm inner diameter loaded 0.15 g catalyst, the fixed bed reactor with a 30 mm inner diameter loaded 60 g catalyst and the single tube fixed bed reactor with an 80 mm inner diameter loaded 2.5 kg catalyst.

Typically, the evaluation operations are conducted with the following procedures. 0.15 g catalyst was weighed and filled in the silica tube. By continuously feeding $N_2$, the catalyst was heated at 120 ºC and dried for 15 min. Activation was started by feeding HCl at 180 ºC for 15 min. Both GHSV of $N_2$ and HCl were selected as 120 $h^{-1}$ (volume based). The reaction was carried out after activation at 1atm and 180 ºC. The reactants were fed with a mixed flow comprising $HCl:C_2H_2:H_2$=1.1:1.0:0.083 with 1200 $h^{-1}$ GHSV of $C_2H_2$. It should be noted that the feeding time of $N_2$ and HCl in plant trial and GHSV of $C_2H_2$ were determined according to the evaluation scale.

### Analysis and Characterization

The catalytic activity and selectivity of catalyst were evaluated by conversion of $C_2H_2$ collected at the outlet of the reactor, and the product was sampled per 15 min, which was analysed via gas chromatography (GC, Tianmei, GC-7890T). The column was selected from Beijing Analysis Instrument Co., limited with the type of GDX-301. The selectivity of VCM was monitored by the FID through a capillary column (Agilent, DB-1) each hour. SEM (JEOL JSM-7401, at 3.0 kV) and TEM (JEOL JEM-2010, at 120.0 kV) were utilized to examine the micromorphology and detailed structures of catalyst before and after the reaction. The Brunauer–Emmett–Teller (BET) specified surface area of the samples were measured by $N_2$ adsorption/desorption at liquid-$N_2$ temperature using Autosorb-IQ2-MP-C system. Before measurements, the sample was degassed at 300 °C until a manifold pressure of 2 mmHg was reached. The elemental composition and chemical state of elements was analyzed by XPS (ESCALAB 250Xi, Al Kα source). XRD (D8 ADVANCE Diffractometer) was applied to reveal information about the crystal structure, chemical composition, and physical properties of the compositions. To further understand the element composition in the catalyst, ICP-OES (IRIS Intrepid II XSP) was employed.

### DFT study methods

All calculations were carried out by the Gaussian 03 program package.[40, 55] The geometrical optimizations of the reactants, products, intermediates and transition states were performed by Beeke's three-parameter exchange functional,[56] the nonlocal correlation functional of Lee, Yang, and Parr[57] (B3LYP) with 6-31G(d) basis set for all atoms except for Au, which was described by Lanl2dz *pseudo*-potential basis set. Harmonic vibrational frequency calculations were performed at the same level in order to confirm various stationary points as either a minimum or a transition structure (TS). Intrinsic reaction coordinate (IRC)[58, 59] calculations were carried out to confirm the connection of each TS to its corresponding reactants and products. All charge analyses reported were calculated by natural bond orbital (NBO) analysis.[60] The discussed energies are relative Gibbs free energies ($\Delta G_{453.15K}$) under reaction conditions. The relative enthalpies ($\Delta H_{453.15K}$) and ZPE corrected electronic energies ($\Delta E_{0K}$) are also provided for reference.

## Acknowledgements

This work was supported by the Natural Scientific Foundation of China (No.736004), the Ministry of Science and Technology of China (Project No.2008BAB41B02) and the National High Technology Research and Development Program of China (Project No.2012AA062901). We also greatly appreciate help on plant trial support from Mr. Jiangkun Si, Mr. Wenhu Hu and Mr. Rui Xia, and the help on DFT study supported by Ms. Silei Xiong from the School of Chemical Engineering, Purdue University, U.S..

## Notes and references

[a] Beijing Key Laboratory of Green Chemical Reaction Engineering and Technology, Department of Chemical Engineering, Tsinghua University, Beijing 100084, China.
[b] Tianye (Group) Co., Ltd. Shihezi, Xinjiang, 832000, China.
* To whom correspondence may be addressed. Tel.: +86-10- 62788994. Fax: +86-10-62772051. E-mail: luoguoh@tsinghua.edu.cn; wf-dce@tsinghua.edu.cn.

Electronic Supplementary Information (ESI) available: [details of any supplementary information available should be included here]. See DOI: 10.1039/b000000x/

1. A. Gennadios, M. A. Hanna and L. B. Kurth, *Lebensmittel-Wissenschaft and Technologie*, 1997, **30**, 337-350.
2. J. Bing and C. Li, *Polyvinyl Chloride*, 2011, **39**, 1-8.
3. G. J. Hutchings and R. Joffe, *Appl Catal*, 1986, **20**, 215-218.
4. G. J. Hutchings, *Catal Today*, 2002, **72**, 11-17.
5. M. Conte, C. J. Davies, D. J. Morgan, T. E. Davies, A. F. Carley, P. Johnston and G. J. Hutchings, *Catal Sci Technol*, 2013, **3**, 128-134.
6. G. J. Hutchings, *Top Catal*, 2008, **48**, 55-59.
7. M. Conte, C. J. Davies, D. J. Morgan, T. E. Davies, D. J. Elias, A. F. Carley, P. Johnston and G. J. Hutchings, *J Catal*, 2013, **297**, 128-136.
8. A. S. K. Hashmi and M. Buehrle, *Aldrichimica Acta*, 2010, **43**, 27-33.
9. M. Zhu, L. Kang, Y. Su, S. Zhang and B. Dai, *Can J Chem*, 2013, **91**, 120-125.
10. H. Zhang, B. Dai, X. Wang, W. Li, Y. Han, J. Gu and J. Zhang, *Green Chem*, 2013, **15**, 829-836.
11. G. J. Hutchings, *J Catal*, 1985, **96**, 292-295.
12. B. Nkosi, N. J. Coville, G. J. Hutchings, M. D. Adams, J. Friedl and F. E. Wagner, *J Catal*, 1991, **128**, 366-377.
13. B. Nkosi, N. J. Coville and G. J. Hutchings, *J Chem Soc Chem Commun*, 1988, 71-72.
14. B. Nkosi, N. J. Coville and G. J. Hutchings, *Appl Catal*, 1988, **43**, 33-39.
15. K. Zhou, J. C. Jia, X. G. Li, X. D. Pang, C. H. Li, J. Zhou, G. H. Luo and F. Wei, *Fuel Process Technol*, 2013, **108**, 12-18.
16. S. J. Wang, B. X. Shen and Q. L. Song, *Catal Lett*, 2010, **134**, 102-109.
17. X. Li, X. Pan and X. Bao, *J Energ Chem*, 2014, **23**, 131-135.
18. X. Li, Y. Wang, L. Kang, M. Zhu and B. Dai, *J Catal*, 2014, **311**, 288–294.
19. K. Zhou, B. Li, Q. Zhang, J. Q. Huang, G. L. Tian, J. C. Jia, M. Q. Zhao, G. H. Luo, D. S. Su and F. Wei, *ChemSusChem*, 2014, **7**, 723-728.
20. X. Li, X. Pan, L. Yu, P. Ren, X. Wu, L. Sun, F. Jiao and X. Bao, *Nat Commun*, 2014, DOI: 10.1038/ncomms4688.
21. K. Zhou, W. Wang, F. Wei, J. K. Si, C. H. Li and J. Zhou, CN102631942, 2012.
22. X. Zhang, H. Shi and B.-Q. Xu, *J Catal*, 2011, **279**, 75-87.
23. A. S. K. Hashmi and G. J. Hutchings, *Angew Chem Int Ed*, 2006, **45**, 7896-7936.
24. C. Marco and H. Graham, *Modern Gold Catalyzed Synthesis*, Wiley-VCH Verlag GmbH & Co. KGaA, 2012.
25. R. J. H. Grisel, P. J. Kooyman and B. E. Nieuwenhuys, *J Catal*, 2000, **191**.
26. M. Haruta and M. Date, *Appl Catal A-Gen*, 2001, **222**.
27. A. Wittstock, V. Zielasek, J. Biener, C. M. Friend and M. Baeumer, *Science*, 2010, **327**.
28. N. Yi, R. Si, H. Saltsburg and M. Flytzani-Stephanopoulos, *Energ Environ Sci*, 2010, **3**.
29. X. Zhang, H. Shi and B. Q. Xu, *J Catal*, 2011, **279**, 75-87.
30. M. Haruta, T. Kobayashi, H. Sano and N. Yamada, *Chem Lett*, 1987, 405-408.
31. R. M. Finch, N. A. Hodge, G. J. Hutchings, A. Meagher, Q. A. Pankhurst, M. R. H. Siddiqui, F. E. Wagner and R. Whyman, *Phy Chem Chem Phys*, 1999, **1**, 485-489.
32. N. Dimitratos, J. A. Lopez-Sanchez and G. J. Hutchings, *Top Catal*, 2009, **52**.
33. B. K. Min and C. M. Friend, *Chem Rev*, 2007, **107**.
34. L. Prati, P. Spontoni and A. Gaiassi, *Top Catal*, 2009, **52**.
35. B. Nkosi, M. D. Adams, N. J. Coville and G. J. Hutchings, *J Catal*, 1991, **128**, 378-386.
36. S. A. Mitchenko, E. V. Khomutov, A. A. Shubin and I. P. Beletskaya, *Kinet Catal*, 2004, **45**, 391-393.
37. K. Shinoda, *Chem Lett*, 1975, 219-220.
38. M. Conte, A. F. Carley, G. Attard, A. A. Herzing, C. J. Kiely and G. J. Hutchings, *J Catal*, 2008, **257**, 190-198.
39. H. Zhang, B. Dai, X. Wang, L. Xu and M. Zhu, *J Ind Eng Chem*, 2012, **18**, 49-54.
40. J. Zhang, Z. He, W. Li and Y. Han, *Rsc Adv*, 2012, **2**, 4814-4821.
41. F. Liu, F. Wei, G. L. Li, Y. Cheng, L. Wang, G. H. Luo, Q. Li, Z. Qian, Q. Zhang and Y. Jin, *Ind Eng Chem Res*, 2008, **47**, 8582-8587.
42. X. B. Wei, H. B. Shi, W. Z. Qian, G. H. Luo, Y. Jin and F. Wei, *Ind Eng Chem Res*, 2009, **48**, 128-133.
43. J. J. Jia, X. G. Li, G. H. Luo, K. Zhou and F. Wei, *Chin J Process Eng*, 2012, **12**, 510-515.
44. C. L. Bracey, P. R. Ellis and G. J. Hutchings, *Chem Soc Rev*, 2009, **38**, 2231-2243.
45. S. Wang, B. Shen and Q. Song, *Catal Lett*, 2010, **134**, 102-109.
46. M. Conte, A. F. Carley, G. Attard, A. A. Herzing, C. J. Kiely and G. J. Hutchings, *J Catal*, 2009, **266**, 164-164.
47. Q. Fu, H. Saltsburg and M. Flytzani-Stephanopoulos, *Science*, 2003, **301**, 935-938.
48. C. N. R. Rao, V. Vijayakrishnan, H. N. Aiyer, G. U. Kulkarni and G. N. Subbanna, *J Phys Chem*, 1993, **97**, 11157-11160.
49. T. Matsumoto, P. Nickut, T. Sawada, H. Tsunoyama, K. Watanabe, T. Tsukuda, K. Al-Shamery and Y. Matsumoto, *Surf Sci*, 2007, **601**, 5121-5126.
50. T. V. Choudhary and D. W. Goodman, *Top Catal*, 2002, **21**, 25-34.
51. M. Kozlowski, *Fuel*, 2004, **83**, 259-265.
52. R. Pietrzak, T. Grzybek and H. Wachowska, *Fuel*, 2007, **86**, 2616-2624.
53. G. Gryglewicz, P. Wilk, J. Yperman, D. V. Franco, Maes, II, J. Mullens and L. C. VanPoucke, *Fuel*, 1996, **75**, 1499-1504.
54. M. Conte, A. F. Carley, C. Heirene, D. J. Willock, P. Johnston, A. A. Herzing, C. J. Kiely and G. J. Hutchings, *J Catal*, 2007, **250**, 231-239.
55. M. J. Frisch, Gaussian, Inc., Pittsburgh, PA, 2004.
56. A. D. Becke, *J Chem Phys*, 1993, **98**, 5648-5652.
57. C. T. Lee, W. T. Yang and R. G. Parr, *Phys Rev B*, 1988, **37**, 785-789.
58. C. Gonzalez and H. B. Schlegel, *J Chem Phy*, 1989, **90**, 2154-2161.
59. C. Gonzalez and H. B. Schlegel, *J Phys Chem*, 1990, **94**, 5523-5527.
60. E. D. Glendening, J. K. Badenhoop, A. E. Reed, J. E. Carpenter and F. Weinhold, *NBO 4.M*, Universityof Wisconsin, Madison, WI, Theoretical Chemistry Institute, 1999.



 